Reliability of organic light-emitting diodes in low-temperature environment

Saihu Pan(潘赛虎), Zhiqiang Zhu(朱志强), Kangping Liu(刘康平), Hang Yu(于航), Yingjie Liao(廖英杰), Bin Wei(魏斌), Redouane Borsali, and Kunping Guo(郭坤平)

Citation: Chin. Phys. B, 2020, 29 (**12**): 128503. DOI: 10.1088/1674-1056/abc154
Journal homepage: http://cpb.iphy.ac.cn; http://iopscience.iop.org/cpb

What follows is a list of articles you may be interested in

Water-based processed and alkoxide-based processed indium oxide thin-film transistors at different annealing temperatures

Xu-Yang Li(栗旭阳), Zhi-Nong Yu(喻志农), Jin Cheng(程锦), Yong-Hua Chen(陈永华), Jian-She Xue(薛建设), Jian Guo(郭建), Wei Xue(薛唯)

Chin. Phys. B, 2018, 27 (**4**): 048504. DOI: 10.1088/1674-1056/27/4/048504

Simulation and experimental study of a novel bifacial structure of silicon heterojunction solar cell for high efficiency and low cost

Haibin Huang(黄海宾), Gangyu Tian(田罡煜), Lang Zhou(周浪), Jiren Yuan(袁吉仁), Wolfgang R. Fahrner, Wenbin Zhang(张闻斌), Xingbing Li(李杏兵), Wenhao Chen(陈文浩), Renzhong Liu(刘仁中)

Chin. Phys. B, 2018, 27 (**3**): 038502. DOI: 10.1088/1674-1056/27/3/038502

Ultra-low temperature radio-frequency performance of partially depleted silicon-on-insulator n-type metal-oxide-semiconductor field-effect transistors with tunnel diode body contact structures

Kai Lu(吕凯), Jing Chen(陈静), Yuping Huang(黄瑜萍), Jun Liu(刘军), Jiexin Luo(罗杰馨), Xi Wang(王曦)

Chin. Phys. B, 2016, 25 (**11**): 118503. DOI: 10.1088/1674-1056/25/11/118503

Evaluation of a gate-first process for AlGaN/GaN metal-oxide-semiconductor heterostructure field-effect transistors with low ohmic annealing temperature

Liuan Li(李柳暗), Jiaqi Zhang(张家琦), Yang Liu(刘扬), Jin-Ping Ao(敖金平)

Chin. Phys. B, 2016, 25 (**3**): 038503. DOI: 10.1088/1674-1056/25/3/038503

GaSb p-channel metal-oxide-semiconductor field-effect transistor and its temperature dependent characteristics

Zhao Lian-Feng, Tan Zhen, Wang Jing, Xu Jun

Chin. Phys. B, 2015, 24 (**1**): 018501. DOI: 10.1088/1674-1056/24/1/018501

RAPID COMMUNICATION

Reliability of organic light-emitting diodes in low-temperature environment*

Saihu Pan(潘赛虎)[1], Zhiqiang Zhu(朱志强)[1], Kangping Liu(刘康平)[2], Hang Yu(于航)[1], Yingjie Liao(廖英杰)[2], Bin Wei(魏斌)[2], Redouane Borsali[3], and Kunping Guo(郭坤平)[2,4,†]

[1] *School of Microelectronics and Control Engineering, Changzhou University, Changzhou* 213164, *China*

[2] *School of Mechatronic Engineering and Automation, Key Laboratory of Advanced Display and System Applications, Ministry of Education, Shanghai University, Shanghai* 200072, *China*

[3] *Universdity of Grenoble Alpes, CNRS, CERMAV, F-*38000 *Grenoble, France*

[4] *London Centre for Nanotechnology, University College London, London WC1H 0AH, UK*

(Received 4 August 2020; revised manuscript received 8 September 2020; accepted manuscript online 15 October 2020)

Organic light-emitting diode (OLED) is an electroluminescent technology that relies on charge-carrier dynamics and is a potential light source for variable environmental conditions. Here, by exploiting a self-developed low-temperature testing system, we investigated the characteristics of hole/electron transport, electro-optic conversion efficiency, and operation lifetime of OLEDs at low-temperature ranging from −40 °C to 0 °C and room temperature (25 °C). Compared to devices operating at room temperature, the carrier transport capability is significantly decreased with reducing temperature, and especially the mobility of the hole-transporting material (HTM) and electron-transporting material (ETM) at −40 °C decreases from 1.16×10^{-6} cm^2/V·s and 2.60×10^{-4} cm^2/V·s to 6.91×10^{-9} cm^2/V·s and 1.44×10^{-5} cm^2/V·s, respectively. Indeed, the temperature affects differently on the mobilities of HTM and ETM, which favors unbalanced charge-carrier transport and recombination in OLEDs, thereby leading to the maximum current efficiency decreased from 6.46 cd·A^{-1} at 25 °C to 2.74 cd·A^{-1} at −40 °C. In addition, blue fluorescent OLED at −20 °C has an above 56% lifetime improvement (time to 80% of the initial luminance) over the reference device at room temperature, which is attributed to efficiently dissipating heat generated inside the device by the low-temperature environment.

Keywords: organic light-emitting diodes (OLEDs), low temperature, reliability, operation lifetime

PACS: 85.60.Jb, 78.60.Fi, 07.20.Mc, 81.40.Rs **DOI:** 10.1088/1674-1056/abc154

1. Introduction

Ambient temperature is an important factor affecting the reliability of organic optoelectronic devices. To date, the significant researches on the reliability of organic optoelectronic devices for high temperature applications have made remarkable progress.[1–6] Recent reports suggest that most organic semiconductor materials are prone to be aged in high-temperature condition, arising from the change of mechanical stress due to the thermal expansion of organic materials.[7] Given their potential impact on the electroluminescent device, adopting organic semiconductors with high glass transition temperature as the functional layer is usually considered crucial to improve the thermal stability of organic light-emitting diodes (OLEDs),[8,9] while other efforts are being dedicated to via using the doped hole transport layer (HTL),[10–13] or introducing the electrode buffer layer to increase the thermal resistance of the devices.[14–16]

Interestingly, with the broadening applications field of OLEDs, there are emerge issues for the specific applications of OLED light sources in diverse and harsh natural environments, especially in extreme low-temperature conditions such as north and south poles, as well as deep seas. To fulfil commercial aspirations, the development of OLEDs cannot overlook the reliability aspect of low temperature. It is important to note that the low-temperature condition is rarely proposed but potentially impairs the reliability of OLEDs. For example, Berleb *et al.*[17] demonstrated low-temperature dependence of carrier transport in conducting polymers. Guan *et al.*[18] reported the transient response of tris (8-hydroxyquinoline) aluminum-based OLEDs at low-temperature. Both examples constitute the current study of low temperature on the OLED performance. However, the dynamic change in electroluminescence properties and device durability of OLEDs operating in different low-temperature conditions is not clear.

In this paper, the charge-carrier dynamics, electro-optic conversion efficiency, and device lifetime of OLEDs under different low temperatures were investigated based on a self-developed low-temperature testing system. We demonstrated that both the hole and electron mobilities in single carrier devices were significantly reduced with the decreasing tem-

*Project supported by the National Natural Science Foundation of China (Grant Nos. 61775130 and 11974236), the Science and Technology Commission of Shanghai Municipality Program, China (Grant Nos. 19DZ2281000 and 17DZ2281000), and the Research Innovation Program for College Graduates of Jiangsu Province, China (Grant Nos. KYCX20_2545 and KYCX20_2549).

†Corresponding author. E-mail: gkp@shu.edu.cn

perature, which thus leads to an unbalanced carrier transport and recombination in OLEDs, ultimately causing a reduction of the current efficiency (*CE*). Furthermore, the lifetime of blue fluorescent devices was characterized by different low-temperature conditions. An above 56% lifetime improvement (time to 80% of the initial luminance) was achieved by the device at −20 ℃ over the one at room temperature.

2. Experiment

2.1. Materials

All the chemicals and regents were used as received from the commercial sources without further purification. The auxiliary materials for OLED fabrication such as HAT-CN (1,4,5,8,9,11-hexaazatriphenylenehexacarbonitrile), TAPC (4,4′-cyclohexylidenebis [N, N-bis(4-methylphenyl) benzenamine]), NPB (N,N′-bis(1-naphthyl)-N,N′-diphenyl-[1,1′-biphenyl]-4, 4′-diamine), ADN (9,10-di(naphth-2-yl)anthracene), DSA-Ph (*p*-bis(p-N,N-diphenyl-aminostyryl)-benzene), TmPyPb (1,3,5-tri(m-pyrid-3-yl-phenyl)benzene), Bphen (4,7-diphenyl-1,10-phenanthroline), and Liq (8-hydroxyquinolatolithium) were purchased from Sigma-Aldrich.

2.2. Device fabrication and characterization

For single charge devices, 200 nm thick NPB and 90 nm thick Bphen were used to fabricate hole- and electron-only devices, respectively, for their carrier transport properties at different low temperatures. The structure of the hole-only device is ITO/MoO_3 (5 nm)/NPB (200 nm)/MoO_3 (5 nm)/Al (100 nm), while the electron-only device is ITO/Bphen: 10 wt% Cs_2CO_3 (30 nm)/Bphen (60 nm)/Liq (1 nm)/Al. From a manufacturing point of view, both NPB and Bphen are relatively low cost but typical transport materials in OLEDs. In contrast, aiming to reveal the influence of the low temperature on the electroluminescence performance, stable and high-efficiency OLEDs are necessary, in case that the spectrometer is unable to detect the EL signal when OLED is significantly affected by low temperature. However, an efficient OLED requires well-balanced carrier transport and optimal energy level matching. In our previous reports,[19–22] the adoption of TAPC and TmPyPb is considered crucial to improve the EL properties in OLEDs. Within this framework, TAPC and TmPyPb instead of NPB and Bphen as transport layers were used in OLEDs. Figure 1 shows the devices architectures of the fluorescent OLEDs (Fig. 1(a)), the corresponding energy-level diagram (Fig. 1(b)), and the molecular structures of the organic materials used in the device (Fig. 1(c)). The fluorescent OLEDs devices with structure of HAT-CN (5 nm)/TAPC (40 nm)/ADN: 3% DSA-Ph (20 nm)/TmPyPb (40 nm)/Liq (1 nm)/Al (100 nm) were fabricated using vacuum evaporation method onto an indium-tin-oxide (ITO) coated glass substrate.

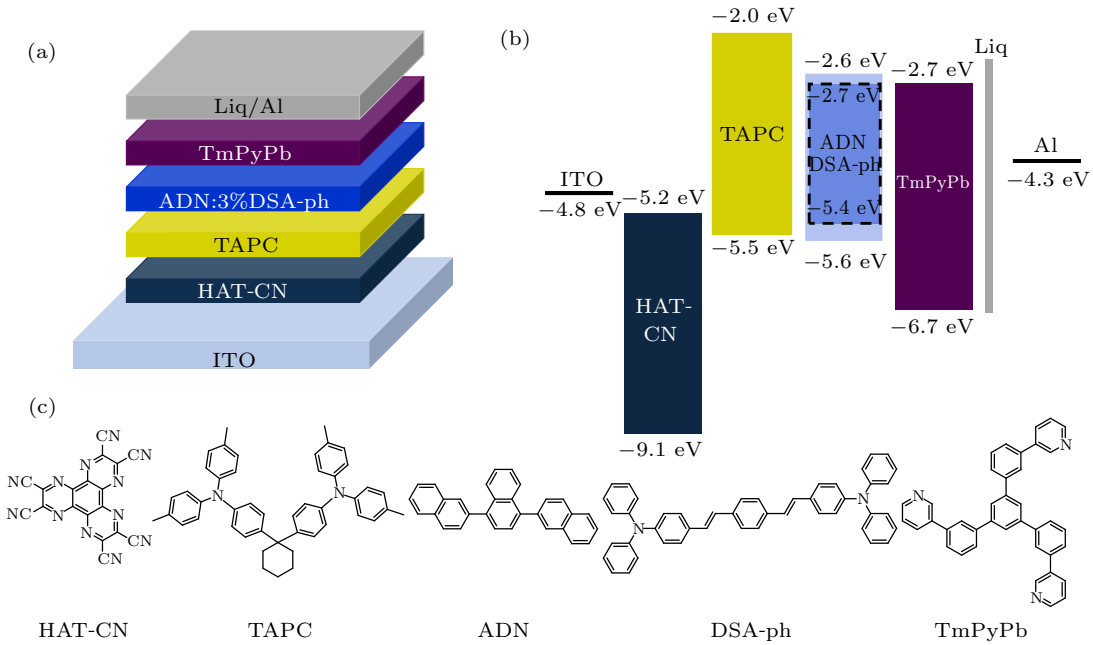

Fig. 1. Fluorescent OLEDs: (a) device architecture of ITO/HAT-CN (5 nm)/TAPC (40 nm)/ADN: 3% DSA-Ph (20 nm)/TmPyPb (40 nm)/Liq (1 nm)/Al (100 nm), (b) energy-level diagram, and (c) molecular structures of the organic materials used in the devices.

The preparation process is as follows. Pre-patterned ITO substrates were successively cleaned with detergent, deionized water, acetone, and isopropanol in an ultrasonic bath, and dried at 80 ℃ for 12 min in an oven. The cleaned ITO substrate was exposed to UV ozone for 30 min, and then immediately transferred to a high-vacuum chamber, and the organic functional layers and the Al top electrode were evaporated layer by layer under a base pressure lower than 1×10^{-5} Pa. Single carrier devices including the hole-only and electron-only devices were further prepared to investigate the mobility

of electrons and holes by space-charge-limit-current (SCLC) method. The current density–voltage–luminescence (J–V–L) characteristics of the devices were measured using Keithley 2400 source meter and PR 650 SpectraScan Colorimeter. The luminance and spectra of each device were measured in the direction perpendicular to the glass substrate.

The composition of the low-temperature testing system is shown in Fig. 2. The system can be divided into three parts: low-temperature vacuum control system, power supply, and photoelectric signal acquisition system. After placing and fixing the sample, the user transfers the sample into the vacuum chamber and starts evacuating until the base pressure reaches 10^{-1} Pa. Liquid nitrogen is slowly injected into the specific liquid nitrogen chamber. And the temperature of the vacuum chamber is able to regulate by using an external temperature controller. When the temperature of the chamber is stable, the OLED device is driven via the external Keithley 2400 source meter. At the same time, one connects the spectrometer with the quartz window outside the vacuum chamber and adjusts the focus point between the spectrometer and sample. If the stable temperature inside the chamber needs to be maintained for about 10 min, then manually supplementing liquid nitrogen to achieve a stable temperature is required during the measurement.

In particular, the low-temperature testing system of the experimental chamber was designed according to the principle of leakage thermostat, where a thermal interface unit controls the heating power and balances the thermal conductivity of liquid nitrogen to meet a stable intermediate temperature. The schematic diagram of the thermostat is shown in Fig. S1(a). The sample holder S was made of red copper, which was connected with a copper rod A with high thermal conductivity and low heat sink properties. And the other end of A was directly connected to the liquid nitrogen chamber. Importantly, a heater integrated with a microcontroller unit (MCU) was installed on the back of the junction between A and S. The specific working process is as follows. (i) The low-temperature heat source from the liquid nitrogen chamber is transferred to A, and a temperature gradient distribution gradually forms. (ii) When the S is stimulated by the heat transfer on A, the MCU collects the real-time temperature by a thermocouple and thus adjusts the heating current via the negative feedback control. (iii) Running the experimental test when S reaches the set temperature and stable distribution.

Furthermore, the working process of the temperature controller is shown in Fig. S1(b). User firstly sets the temperature required for the experiment via the panel keys and the digital tube module, and the feedback voltage from a thermocouple is detected by the internal MCU to achieve the real-time temperature control of the sample holder. Indeed, the MCU module contains a proportional-integral-derivative (PID) controller, which depends on the deviation $e(t)$ between the given temperature $r(t)$ and the feedback temperature $y(t)$ for setting modulation time t of the target temperature. And then MCU outputs the current by using the silicon-controlled rectifier (SCR) module, resulting in the electrical resistance heating (ERH) to generate heat, ultimately causing thermal exchange with the copper rod to transfer to the sample holder. In the meantime, the feedback voltage from a thermocouple of the sample holder can be recognized by the MCU detection circuit, thereby maintaining the stable temperature.

Fig. 2. OLEDs low-temperature testing system.

3. Results and discussion

We firstly studied the low-temperature dependence of carrier transport properties in typical organic functional layers. The J–V characteristic curves of the hole-only and electron-only devices at different low temperatures ranging from room temperature (25 ℃) to ultra-low-temperature (−40 ℃) are shown in Fig. 3. It is clearly observed that both hole and electron currents in the single-carrier devices gradually decreased with reducing temperature. For the hole-only devices,

the current density was less affected by the reduced temperature in the case of low-temperature change from 25 ℃ to −10 ℃. With the further reduction of ambient temperature, the current density of the hole-only device dramatically decreased, particularly at the temperature of −40 ℃. At the same voltage of 9 V, the hole-devices reached current densities of 205.39 mA·cm^{-2}, 161.22 mA·cm^{-2}, 114.44 mA·cm^{-2}, 40.41 mA·cm^{-2}, and 11.58 mA·cm^{-2} at the ambient temperatures of 25 ℃, 0 ℃, −10 ℃, −20 ℃, and −40 ℃, respectively. Notably, the current density for the device operating at −40 ℃ is only ∼ 5% of that at room temperature. Similarly, for the same current density of 205.39 mA·cm^{-2}, the driving voltages were 9.0 V, 9.4 V, 9.9 V, 11.1 V, and 13.7 V for the devices operating at low temperatures of 25 ℃, 0 ℃, −10 ℃, −20 ℃, and −40 ℃, respectively. It is therefore reasonable to assume that the hole-only devices under the low-temperature environment need a higher electric field to achieve the same current density with respect to the device operating at room temperature.

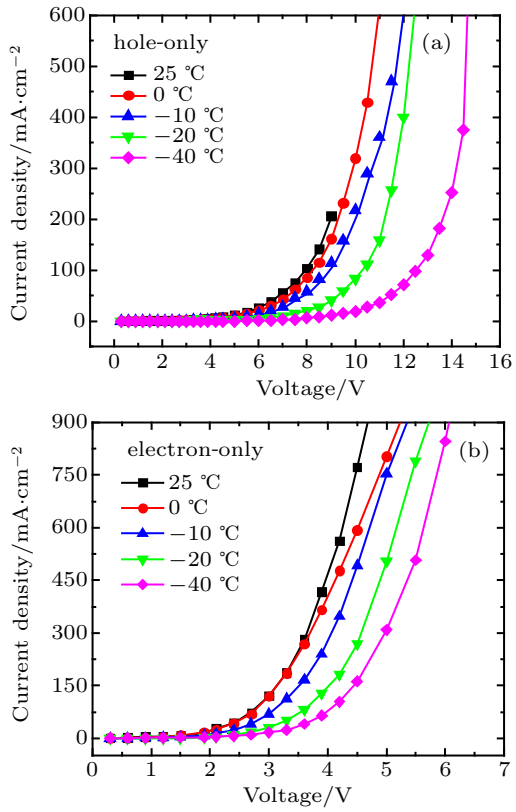

Fig. 3. The *J*–*V* characteristic curves of the single carrier devices at the temperatures of 25 ℃, 0 ℃, −10 ℃, −20 ℃, and −25 ℃: (a) hole-only devices and (b) electron-only devices.

Figure 3(b) depicts the *J*–*V* properties of the electron-only devices at different low temperatures, a similar decreasing trend of the current density is observed in the devices with reducing temperatures. Nevertheless, the current density of the electron-only devices did not show a significant difference when the ambient temperature reduced from 25 ℃ to 0 ℃. Another interesting character is that all electron-only devices exhibited relatively lower driving voltage with respect to the voltage in the hole-only devices. The main reason for such a feature probably derives from the intrinsic property of organic semiconductor materials, which limits the charge-carrier mobility in devices at different temperatures, and therefore affecting the current density.

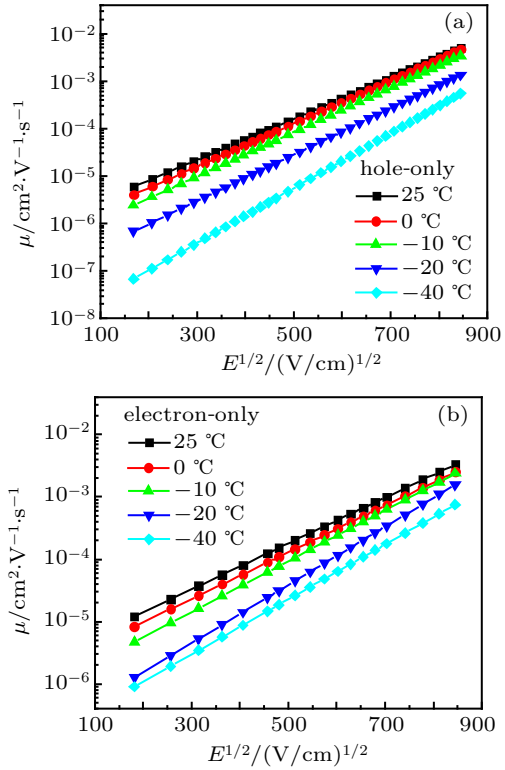

Fig. 4. Single carrier devices in different electric field at the temperatures of 25 ℃, 0 ℃, −10 ℃, −20 ℃, and −25℃: (a) hole mobility of the hole-only devices, and (b) electron mobility of the electron-only devices.

The mobility of organic materials is an important parameter, which generally determines the power consumption of device and the carrier migration speed under certain electric field.[23] Hence, space charge limiting current (SCLC) method is used to evaluate the carrier mobility of the hole-only and electron-only devices at different ambient temperatures of 25 ℃, 0 ℃, −10 ℃, −20 ℃, and −40 ℃. The *J*–*V* curve of a typical organic material can be generally divided into three regions. The region under high bias is the space charge limited current region,[24] which is described as

$$J = \frac{9}{8}\varepsilon\varepsilon_0\mu\frac{E^2}{L}, \tag{1}$$

where E is the electric field strength, ε and ε_0 are the relative permittivity and free space permittivity, respectively, and L is the thickness of the organic layer in the device. In fact, the carrier mobility is closely related to the electric field strength, which can be expressed by the Poole–Frenkel formula[25]

$$\mu(E) = \mu_0\exp(\gamma\sqrt{E}), \tag{2}$$

where μ_0 is the zero electric field mobility, and γ is the electric field dependence factor. The following formula can be derived

from Eqs. (1) and (2):

$$J = \frac{9}{8}\varepsilon\varepsilon_0\mu\frac{E^2}{L}\mu_0\exp(\gamma\sqrt{E}). \tag{3}$$

Furthermore, taking the logarithm of both sides of Eq. (3), we obtain

$$\ln\left(\frac{J}{E^2}\right) = \ln\left(\frac{9}{8}\frac{\varepsilon\varepsilon_0\mu_0}{L}\right) + \gamma\sqrt{E}, \tag{4}$$

where $\ln\left(J/E^2\right)$ has a linear relationship with $\gamma\sqrt{E}$. According to the slope and intercept of the fitting line, the corresponding carrier mobility μ_0 under zero electric field is calculated, and the carrier mobility $\mu(E)$ under certain electric field can be obtained by Eq. (2).

The fitting results of the single carrier device are shown in Figs. S2 and S3. We report in Fig. 4 the hole and electron mobilities in the single carrier devices at five different temperatures with the electric field. It is important to note here that the carrier mobility of both NPB and Bphen in the single carrier device is less affected by ordinary low-temperatures (0 ℃, −10 ℃), while dramatically decreases for harsh low-temperature environments (−20 ℃ and −40 ℃).

As reported in Table 1, we focus on the hole and electron mobilities under zero-applied electric field at different low temperatures. As the temperature reduced, both hole and electron mobilities in the single carrier devices gradually decreased. In particular, the hole mobility of the device at −40 ℃ is only 6.91×10^{-9} cm^2/V·s, indicating that the harsh low-temperature of −40 ℃ greatly limits the carrier migration capacity of the NPB-based device. For the electron-only devices, the number of free-moving electrons in devices at low-temperature is significantly less than that in devices at room temperature. According to our calculations, the electron mobility of the Bphen-based electron-only device at −40 ℃ reaches 1.44×10^{-5} cm^2/V·s, which is only ∼ 16.7% of the one at room temperature.

Table 1. Summary of the hole and electron mobilities at different low temperatures.

Temperature/℃	25	0	−10	−20	−40
μ_h/(cm^2/V·s)	1.16×10^{-6}	6.94×10^{-7}	3.94×10^{-7}	1.14×10^{-7}	6.91×10^{-9}
μ_e/(cm^2/V·s)	2.60×10^{-4}	1.74×10^{-4}	8.61×10^{-5}	1.82×10^{-5}	1.44×10^{-5}

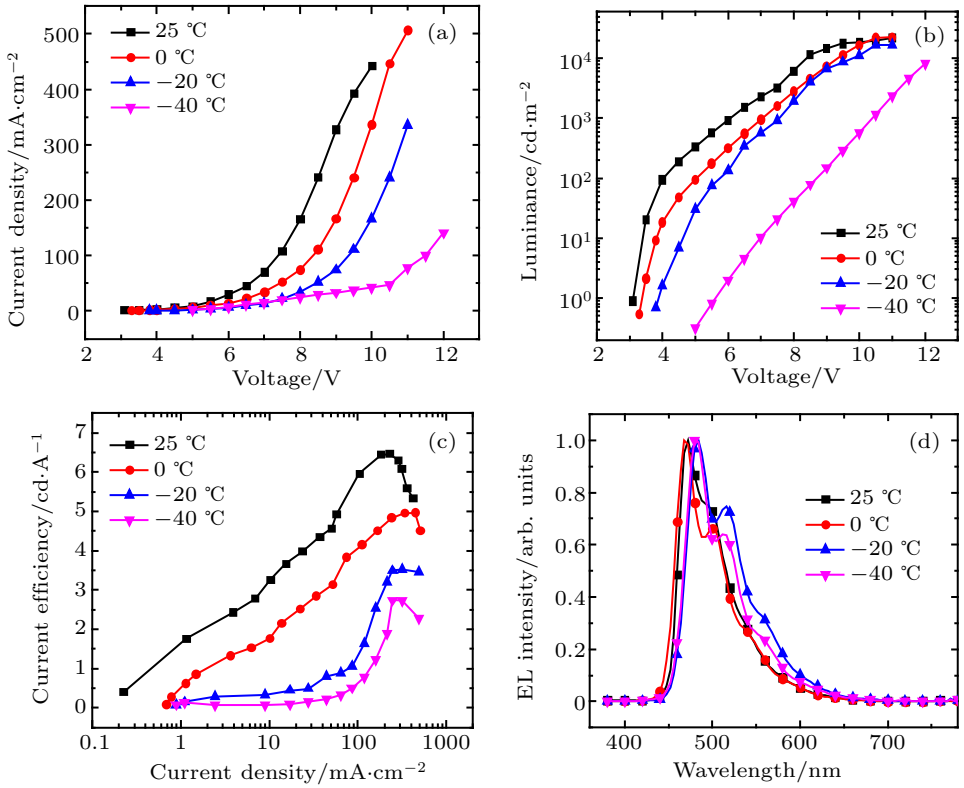

Fig. 5. Fluorescent OLEDs devices at the temperatures of 25 ℃, 0 ℃, −20 ℃, and −40 ℃: (a) *J*–*V* characteristic, (b) *L*–*V* characteristic, (c) *J*–*CE* characteristic, and (d) EL spectrum.

In order to evaluate the electroluminescence (EL) properties of OLEDs at low-temperature and to reveal the influence of the low temperature properties on the device performance, a group of fluorescent OLEDs at different low temperature conditions were tested. For all the fluorescent OLED devices, the typical blue light-emitting molecule DSA-ph was selected as the guest emitter, and ADN was used as the matrix of the emissive layer. Figure 5 shows the device performance of OLEDs at different low temperatures of −40 ℃, −20 ℃, 0 ℃, and 25 ℃. The OLEDs' most significant parameters are summa-

rized in Table S1. From the *J*–*V* curves of the devices at different ambient temperatures in Fig. 5(a), all the test devices exhibit significant diode characteristics. It can be clearly observed that the current density of the device decreases with decreasing ambient temperature. Notably, at a driving voltage of 9 V, the current density of the device at −40 ℃, with a value of 33.23 mA·cm^{-2}, is only 10% of that at room temperature. This is consistent with the above electrical property of the single-carrier devices.

Figure 5(b) illustrates the luminance–voltage (*L*–*V*) curves of OLEDs under different ambient temperature conditions. It clearly suggests that the turn-on voltage of the fluorescent OLEDs devices gradually increases with the decrease of the ambient temperature. The turn-on voltages of the devices at 25 ℃, 0 ℃, −20 ℃, and −40 ℃ were 3.2 V, 3.4 V, 3.9 V, and 4.8 V, respectively. And the maximum luminous of the device at such low temperature reached 22290 cd·m^{-2}, 22785 cd·m^{-2}, 16887 cd·m^{-2}, and 8286 cd·m^{-2}, showing a decreasing trend with low temperature. Figure 5(c) presents the *CE*–*J* characteristic curves of the OLEDs devices in different low-temperature environments. The maximum *CE* of the OLEDs at 25 ℃, 0 ℃, −20 ℃, and −40 ℃ reached 6.46 cd·A^{-1}, 4.97 cd·A^{-1}, 3.51 cd·A^{-1}, and 2.74 cd·A^{-1}, respectively. It is noteworthy that the device at both −20 ℃ and −40 ℃ exhibited low efficiency at all current driving processes, and especially it was the lowest for the device at −40 ℃. It is therefore reasonable to conclude that the extreme low-temperature has a great impact on the efficiency of fluorescent OLEDs. Such a reduction in the device efficiency is due to the decreased levels in the electron/hole dynamic of the diode at low temperature, and therefore causing unbalanced charge-carrier transport, recombination and non-radiative losses.

The normalized EL spectra of OLEDs at different low-temperatures are shown in Fig. 5(d). At ambient temperatures of 25 ℃, 0 ℃, −20 ℃, and −40 ℃, the blue fluorescent devices exhibited EL emission peaked at 472 nm, 468 nm, 484 nm, and 480 nm, respectively. Also, the full width at half maximum slightly increased from 56 nm to 60 nm with reducing low temperature (Table S1). The main reason for this is probably the presence of unbalanced hole and electron transport in devices at low temperature, which results in the change in recombination zone, thereby affecting the EL spectra.[26,27]

We further studied the operation lifetime of the OLED devices at different low temperatures of 25 ℃, 0 ℃, and −20 ℃. For typical fluorescent OLEDs, T_{80} is usually chosen as the comparison index, which refers to the time when the luminescence drops to 80% of the initial luminescence at a constant current density.[28–30] Figure 6 shows the time evolution of the luminance, and the change in voltage from its initial value, $\Delta V = |V(t=0) - V(t)|$, all devices were measured under conditions of vacuum chamber (10^{-1} Pa). The devices were operated at low temperature and at a constant current density for an initial luminance of around 580 cd·m^{-2}. As observed in Fig. 6(a), the luminescence intensity of the devices at all low temperatures shows a rapid decline in the early stage, and then the luminescence degradation becomes slower. These are consistent with the characteristics of the lifetime curve of traditional fluorescent devices.[31,32] Interestingly, the device at −20 ℃ exhibits the best operation lifetime with $T_{80} = 75$ min, which is more than 56% longer than that of device ($T_{80} = 48$ min) at room temperature. Figure 6(b) shows the curves of the device driving voltage increase with time at constant current. Conversely, the ΔV gradually rises with increasing time, and the device at −20 ℃ presents the lowest ΔV at the same degradation process.

The reason for the long operating lifetime can be attributed to the efficiently dissipation of heat generated inside the device through decreased ambient temperature. Although unbalanced charge carrier-induced quenching decreases the device efficiency, Joule heating is a major factor contributing to device degradation.[33] It has been suggested that localized Joule heating can degrade brightness homogeneity and this effect becomes worse as the device temperature increases during long-term operation.[34] The apparently unusual result we report here confirms that the ambient temperature management strategies can be successfully used to facilitate heat dissipation and reduce Joule heating, and thus enhance the device lifetime.

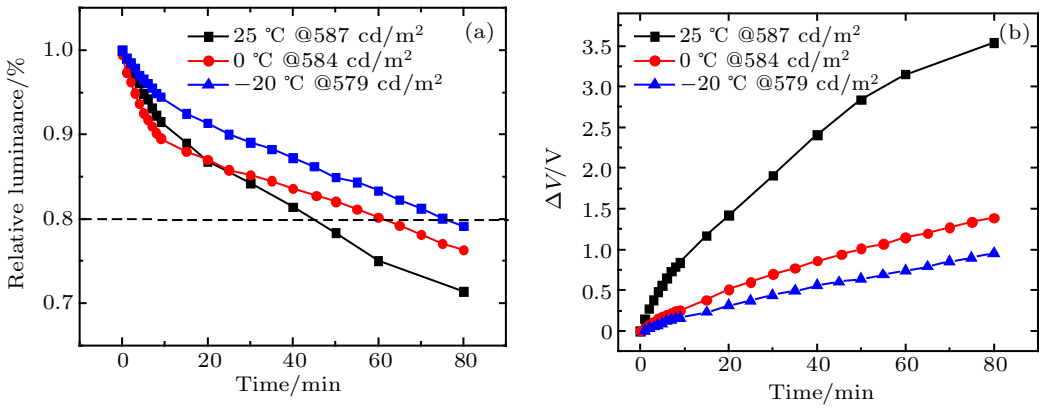

Fig. 6. Fluorescent OLEDs at the temperatures of 25 ℃, 0 ℃, and −20 ℃: (a) normalized luminous versus time, and (b) the change of device operating voltage versus time.

4. Conclusions

This work provides a great advance into the reliability of OLEDs under low-temperature environment. The effects of low-temperature environment on the electrical characteristics of hole- and electron-only devices suggested that the charge mobility of organic semiconductors decreases with reducing temperature. For the blue fluorescent OLEDs, the maximum current efficiency at −40 ℃ was reduced by 41% compared with room temperature (25 ℃) one. Moreover, the EL spectra of devices at different low temperatures were also investigated and discussed. We also showed that the low temperature significantly improved the device lifetime. Crucially, an above 56% lifetime improvement has been successfully achieved by the device at −20 ℃ over the one at room temperature. The next step is clearly to investigate the reliability of phosphorescent OLEDs under low temperature conditions. These thermal management strategies provide a theoretical guidance for material development and OLED applications at low temperature.

References

[1] Kuribara K, Wang H, Uchiyama N, Fukuda K, Yokota T, Zschieschang U, Jaye C F D, Klauk H, Yamamoto T, Takimiya K, Ikeda M, Kuwabara H, Sekitani T, Loo Y L and Someya T 2012 *Nat. Commun.* **3** 723

[2] Zhao W C, Qian D P, Zhang S Q, Li S S, Inganas O, Gao F and Hou J H 2016 *Adv. Mater.* **28** 4734

[3] Ali B A, Moubah R, Boulezhar A and Lassri H 2020 *Chin. Phys. B* **29** 098801

[4] Gao J, Yu Q Q, Zhang J, Liu Y, Jia R F, Han J, Wu X M, Hua Y L and Yin S G 2017 *Chin. Phys. B* **26** 098507

[5] Chen G, Si C F, Tang Z Y, Guo K P, Wang T H, Zhang J H and Wei B 2016 *Synth. Met.* **222** 293

[6] Park J and Kawakami Y 2006 *J. Disp. Technol.* **2** 333

[7] Zufle S, Neukom M T, Altazin S, Zinggeler M, Chrapa M, Offermans T and Ruhstaller B 2015 *Adv. Energy Mater.* **5** 1500835

[8] Chung Y H, Sheng L, Xing X, Zheng L L, Bian M Y, Chen Z J, Xiao L X and Gong Q H 2015 *J. Mater. Chem. C* **3** 1794

[9] Cm K, Kronenberg N M, Murawski C, Yoshida K, Deng Y L, Berz C, Li W B, Wei M J, Idw S and Gather M C 2018 *Adv. Opt. Mater.* **6** 1800496

[10] Park S R, Seo J S, Ahn Y, Jn H L and Suh M C 2018 *Org. Electron.* **63** 194

[11] Kwak J, Lyu Y Y, Noh S, Lee H, Park M, Choi B, Char K and Lee C 2012 *Thin Solid Films* **520** 7157

[12] Huang X L, Zou J H, Liu J Z, Jin G, Li J B, Yao S L, Peng J B, Cao Y and Zhu X H 2018 *Org. Electron.* **58** 139

[13] Kim J H, Chen Y, Liu R and So F 2014 *Org. Electron.* **15** 2381

[14] Xu J J, Wang Y L, Chen Q, Lin Y W, Shan H Q, Val R and Xu Z X 2016 *J. Mater. Chem. C* **4** 7377

[15] Tsang D P K, Matsushima T and Adachi C 2016 *Sci. Rep.* **6** 22463

[16] Zheng L P, Xu J J, Feng Y M, Shan H Q, Fang G J and Xu Z X 2018 *J. Mater. Chem. C* **6** 11471

[17] Berleb S, Mückl A G, Brütting W and Schwoerer M 2000 *Synth. Met.* **111** 341

[18] Yuan C, Guan M, Zhang Y, Li Y Y, Liu S J and Zeng Y P 2017 *Appl. Surf. Sci.* **413** 191

[19] Tao P, Li W L, Zhang J, Guo S, Zhao Q, Wang H, Wei B, Liu S J, Zhou X H and Yu Q 2016 *Adv. Funct. Mater.* **26** 881

[20] Si C F, Li Z F, Guo K P, Lv X, Pan S H, Chen G, Hao Y Y and Wei B 2018 *Dyes Pigm.* **148** 329

[21] Ye Z H, Ling Z T, Chen M Y, Y , J L, W , S L, Zheng Y Q, Wei B, Li C, Chen G and Shi Y 2019 *RSC Adv.* **9** 6881

[22] Pan S H, Liu K P, Ye Y T, Gao X C, Tang Z Y, Ye Z H, Y , N J, Guo K P and Wei B 2020 *Org. Electron.* **78** 105577

[23] Al-Absi M A and As-Sabban I A 2014 *Analog Integr. Circuits Process* **81** 23

[24] Carbone A, Pennetta C and Reggiani L 2009 *Appl. Phys. Lett.* **95** 233303

[25] Pal A J, Osterbacka R, Kallman K M and Stubb H 1997 *Appl. Phys. Lett.* **71** 228

[26] Guo K P, Wang S L, Si C F, Wang T H, Zhang J, Chen C B, Jing Y L, Yang L Q, Chen G and Wei B 2017 *Phys. Status Solidi A* **214** 1600689

[27] Guo K P, Chen C B, Sun C, Peng C Y, Yang L Q, Cai M, Zhang X W and Wei B 2016 *J. Phys. D: Appl. Phys.* **49** 235105

[28] Zhang F L, Si C F, Dong X B, Wei D H, Yang X, Guo K P, Wei B, Li Z Y, Zhang C, Li S Z, Zhai B and Cao G X 2017 *J. Mater. Chem. C* **5** 9146

[29] Zhang Y, Lee J and Forrest S R 2014 *Nat. Commun.* **5** 5008

[30] Guo K P, Li W L, Zhang J H, Zhang X W, Wang X, Chen G, Xu T, Yang L Q, Zhu W Q and Wei B 2016 *RSC Adv.* **6** 55626

[31] Zhang J P, Li W B, Cheng G L, Chen X, Wu H and MHH S 2014 *J. Lumines.* **154** 491

[32] Weaver M S, LA M, Rajan K, MA R, JA S, JJ B, PE B, GL G, ME G, PM M, Hall M, Mast E, Bonham C, Bennett W and Zumhoff M 2002 *Appl. Phys. Lett.* **81** 2929

[33] Zhao L F, Kwangdong R, Sara K, Khaled A K, Samik J, Stephen B, Seth R M, Claire G and Barry P R 2020 *Adv. Mater.* **32** 2000752

[34] Chung S J, Lee J H, Jaewook J, Jang-Joo K and Yongtaek H 2009 *Appl. Phys. Lett.* **94** 253302